Multiple-plane anisoplanatic phase correction in a laboratory digital holography experiment

Abbie E. Tippie* and James R. Fienup

Institute of Optics, University of Rochester, Rochester, New York 14627, USA
**Corresponding author: tippie@optics.rochester.edu*

Received June 4, 2010; revised July 27, 2010; accepted August 19, 2010;
posted September 13, 2010 (Doc. ID 129557); published September 30, 2010

We present results for a digital holography experiment with anisoplanatic image correction through two discrete planes of phase errors. Using a nonlinear optimization technique, we maximize a modified sharpness metric to solve for estimates of the phase errors in the system in the multiple planes where they physically exist. We show that correcting for phase errors in multiple planes gives a superior image to correction in one plane. © 2010 Optical Society of America

OCIS codes: 090.1000, 090.1995, 110.3010, 110.6150.

Anisoplanatic imaging occurs, for example, when the light scattering from two spatially separated object points passes through different portions of the atmosphere (or other aberrating media) on the way to the entrance pupil of an imaging system and, as a result, has significantly different point spread functions across the image of the object. This effect occurs in horizontal path imaging and ground-based astronomy, as well as other applications. Researchers in the astronomy community have attempted multiple guide stars, coupled with adaptive optic systems containing more than one deformable mirror in different axial planes, to overcome some of the effects of anisoplanatism [1]. In coherent imaging with digital holography, Thurman and Fienup showed isoplanatic [2] and anisoplanatic [3] (when the aberrating plane was separated from the entrance pupil) image correction in one plane using a nonlinear optimization, sharpness-metric-based approach. Marron *et al.* demonstrated image correction over a small region of the entire field of view in the presence of anisoplanatic phase errors [4]. We developed an algorithm for estimating phase errors in multiple planes using an image sharpness metric that allows correction over the entire image and demonstrated it in digital simulations [5]. In this Letter, we demonstrate this approach in digital holography laboratory experiments and show the importance of correcting for multiple planes of phase errors when there is more than one plane of phase errors in the system that cause anisoplanatic blurring. By estimating and correcting in the computer the phase errors in the planes in which they occur, we are able to achieve anisoplanatic image correction over the entire field of view.

We performed our experiment using the laboratory digital holography experiment illustrated in Fig. 1. An argon-ion laser operating at a wavelength of 514 nm was used as the coherent illumination source. A beam splitter was used to divide the light between two paths, an off-axis reference beam and a beam to illuminate the object. The laser output power was 400 mW, and the power in the reference arm of the experiment was reduced with a neutral density filter of optical density 5.5 such that the light from the reference beam was moderately brighter than from the diffuse scattering object. In this Letter, we present results for two different imaging cases. The first case is one with a 3.2 cm brass toy train and three 7.9 mm (5/16 in.) ball bearings mounted on a black, low-reflectance felt cloth. In the second case, we removed the ball bearings and imaged the train only.

The object was mounted on a computer-controlled rotation stage and was rotated 2.09 mrad between collection frames. We collected the holographic interference patterns for $K = 9$ speckle realizations using a complementary metal-oxide-semiconductor camera with a 6.7 μm pixel pitch. The camera collected 1024×1280 pixels, but we cropped the data to a 1024×1024 square. We digitally separated the object field by first Fourier transforming the collected intensity data, windowing out the object term, and performing an inverse Fourier transform.

With access to the field from the object obtained through this holographic reconstruction, we can digitally propagate the field to any z plane. We used paraxial angular spectrum propagation, where an arbitrary field $g(x, y)$ can be propagated a distance z by

$$A[z; g(x,y)] = \mathrm{FT}^{-1}\{\mathrm{FT}[g(x,y)] \exp[-i\pi\lambda z(f_x^2 + f_y^2)]\}, \tag{1}$$

where FT denotes a discrete Fourier transform. Angular spectrum propagation preserves the pixel sample spacing regardless of propagation distance. However, with the object being approximately five times larger than the detector, as was the case in this experimental arrangement, the initial 1024×1024 array recorded by the detector would need to be embedded into a much larger array to avoid aliasing artifacts when propagating to the object plane. Multiplying the field in the detector plane by an appropriate converging spherical wave allows for

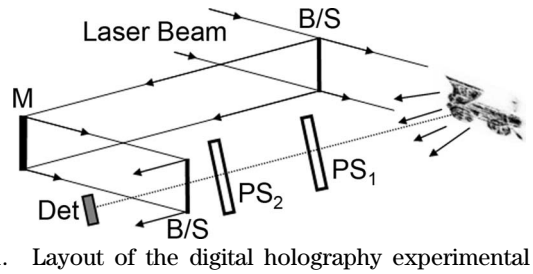

Fig. 1. Layout of the digital holography experimental setup including phase screens: B/S, beamsplitter; M, mirror; Det, detector array, and PS, phase screen.

coordinate transformation to collimated space [6], which allows us to maintain a reasonable array size for large object/detector size ratios.

For static phase screens, we used plastic compact disk cases that were slightly warped by heat treating to increase the aberration. To cause anisoplanatism, two phase screens were separated within the propagation path between the object and detector. The total distance between the object and detector was 3.32 m. One screen (Screen A) was placed 22 cm from the detector, and the other (Screen B) was placed 104.3 cm from the detector. The uncorrected images (corrected just for focusing) when blurred by Screen A are shown in Figs. 2(a) and 2(b), by Screen B in Figs. 2(c) and 2(d), and by both screens in Figs. 2(e) and 2(f). The anisoplanatism introduced by these two phase screens can be seen in the images of the ball bearings, which act like point sources and, therefore, are local point spread functions, below and to the left of the train. In both Figs. 2(c) and 2(e), they are all distinctly different from one another in their details. In contrast, with only Screen A present, Fig. 2(a) shows that all three point sources have similar blur functions, i.e., an approximately isoplanatic case.

To quantify the quality of a given image, we used a modified Muller–Buffington sharpness metric [5,7]:

$$S = \sum_{\xi,\eta} W(\xi,\eta) I^{\beta}(\xi,\eta) - \alpha \sum_{k=1}^{K} \sum_{f_\xi f_\eta} M_k(f_\xi, f_\eta) |F_k(f_\xi, f_\eta)|^2, \tag{2}$$

where $W(\xi,\eta)$ is an optional window function that allows one to select a subregion of the image on which to base the phase-error correction (equal to unity over the entire image unless otherwise stated), $I(\xi,\eta)$ is the incoherent sum of our K speckled images, α and β are constants (we used $\beta = 1.01$ [2]), $M_k(f_\xi, f_\eta)$ is a weighting function defined by the spatial frequency content of the kth speckle realization of the object field sensed over the area of the digital hologram, and $F_k(f_\xi, f_\eta)$ is the Fourier transform of the kth object field in the image plane. M_k was the same for all the speckle realizations. For the first case, with the scene containing both the train and the ball bearings, we used only the first term of this sharpness metric in a nonlinear optimization algorithm [5] to reconstruct the two discrete planes of phase errors present in our optical system and a corrected image. We found the metric to perform well under this imaging condition; the solution for the estimated phase screens was driven in large part by the strong glints produced by the ball bearings in the scene. For the second case in which the ball bearings were removed, we found it necessary to use both terms in this metric to prevent oversharpening of the image. Estimating multiple phase screens in a sharpness-metric nonlinear optimization approach tends to drive the solution to a telescopelike pair of phase screens, demagnifying and warping the image. This effect makes the sharpness metric higher [5], but the image may be a poor reconstruction of the original object. To combat this specific form of oversharpening, the second term in Eq. (2) requires the spatial bandwidth of the field to be the same in the image plane as it is in the detector plane. We infer

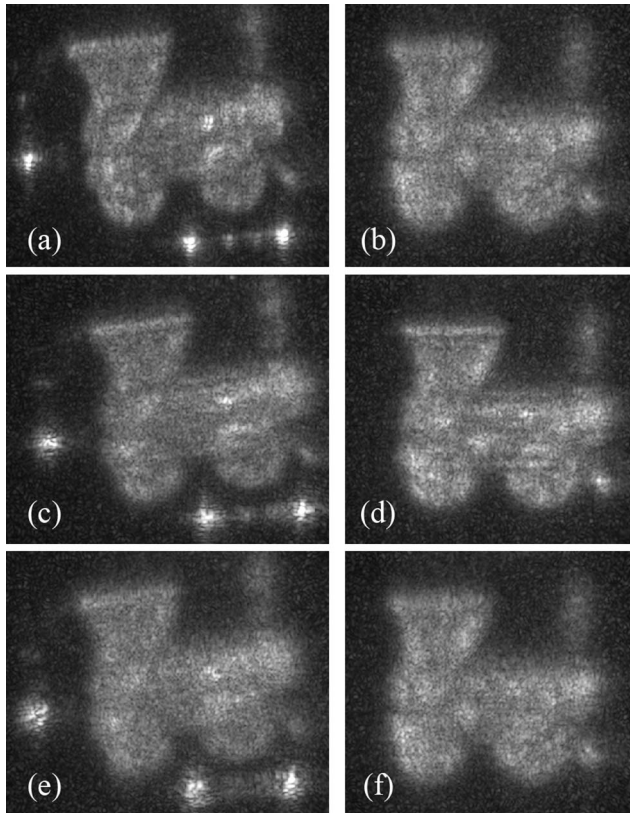

Fig. 2. Image with (a), (b) Screen A, (c), (d) Screen B, and (e), (f) both screens present in the imaging path. Images shown here are scaled, saturated, and cropped to show 530×650 pixels (left column, with ball bearings) and 535×575 pixels (right column, without ball bearings) of the entire 1024×1024 array.

the spatial bandwidth of the object from the Fourier transform of the field in the detector plane. The spatial bandwidth is not changed by free-space propagation and is changed negligibly by the phase screens, allowing us to approximate it everywhere. An analytic gradient for that sharpness metric allows for efficient computation in a conjugate gradient search [5]. For these reconstructions, we employed a bootstrapping approach using the method of sieves [8]. In this approach, we start by convolving a point-by-point version of the analytic gradient with a large Gaussian kernel so that only low-order phase corrections are made. Through successive iterations, we slowly reduce the size of the Gaussian kernel until we eventually solve for the point-by-point phase map reconstruction; this helps to avoid algorithm stagnation. For this work, we started with a Gaussian kernel with a FWHM of 100 pixels and reduced the Gaussian kernel size by half every five iterations. Point-by-point phases were used to better estimate the high-frequency content present in the physical screens. The nonlinear optimization code took 130 min to run on an IBM x3755 server with four AMD Opteron 8224 SE processors. We believe that with more efficient programming and use of graphics processing unit cards, this process would run many times faster.

We also tried single-plane correction in each of several planes – the detector plane, each phase-screen plane, and a few planes located between the two phase screens. For this experiment, we found the best single-plane correction to

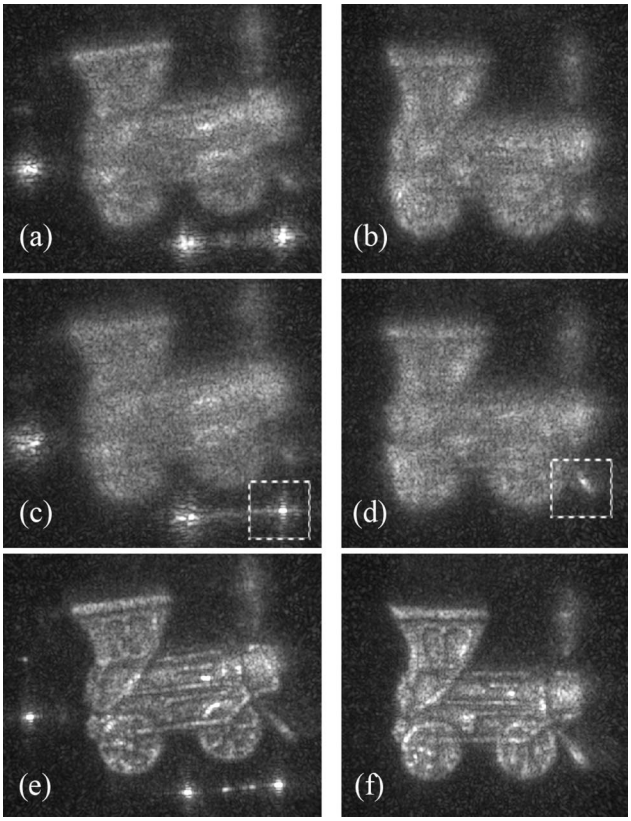

Fig. 3. Comparison of (a), (b) isoplanatic correction across the entire array, (c), (d) isoplanatic correction over a smaller region of the image, indicated by dashed line and (e), (f) anisoplanatic correction of phases in both the planes of Screens A and B. Figures cropped to show 530×650 pixels (left column) and 535×575 pixels (right column) of the entire 1024×1024 array. Images scaled and saturated to bring out details of the dim portions of the objects in addition to bright glints.

be in the plane of phase Screen A, the one closer to the detector. This near-isoplanatic image correction, shown in Figs. 3(a) and 3(b), are a slight improvement upon the uncorrected images shown in Figs. 2(e) and 2(f). We see strong evidence of anisoplanatism still present in the resulting images in Figs. 3(a) and 3(b) because one cannot correct anisoplanatic errors in a plane near the detector. Figures 3(c) and 3(d) show images corrected, using the weighting function $W(\xi, \eta)$ in Eq. (2), over small, isoplanatic patches designated by the dashed regions. The features within this region of interest are sharpened, while the rest of the image remains unimproved. In fact, areas far from the corrected region in Fig. 3(c) are blurred even more than the uncorrected image, similar to what happens with adaptive optics correction for areas of an image outside of the isoplanatic patch surrounding a guide star. Figures 3(e) and 3(f) show the images corrected in both of the planes of the pair of phase screens. In the space-variant correction shown in Fig. 3(e), all three ball bearings have a uniformly tight focus. Furthermore, secondary reflections from the neighboring ball bearings, which are physically present, are clearly visible between the two lower ball bearings, although previously undetectable in the uncorrected case. The details of the train, including the spokes on the wheels and other fine features, are apparent only with this multiple-plane phase-screen correction.

We repeated this experiment after removing the ball bearings, imaging only the toy train. The experimental setup remained the same for both imaging scenarios. The absence of bright, sharp glints in the object makes it more difficult for the image sharpening algorithm. As previously mentioned, we used the modified sharpness metric of Eq. (2). The algorithm was able to correct the anisoplanatic errors to produce a much sharper image, shown in Fig. 3(f), despite having no strong point scatterers.

We have successfully demonstrated anisoplanatic correction of two static phase screens in a laboratory digital holography experiment using an image sharpening algorithm. The corrected images were much sharper than the best single-plane correction case, even when the object contained no prominent point scatterers. We found it was necessary to add a term to the sharpness metric to avoid oversharpening of the image by demagnification. The approach is applicable to correcting any number of phase screens and should be applicable to a continuous 3D volume of turbulence, although its performance will undoubtedly suffer with an increasing number of unknown phase parameters. Further research will be needed to determine the number of, and complexity of, phase screens that can be successfully corrected for a given type of object (we expect it to depend on the object's space-bandwidth product, contrast, and spatial structure, for example) and signal-to-noise ratio.

We thank Richard Marron for producing the phase screens used in these experiments.

References

1. D. C. Johnston and B. M. Welsh, J. Opt. Soc. Am. A **11**, 394 (1994).
2. S. T. Thurman and J. R. Fienup, J. Opt. Soc. Am. A **25**, 983 (2008).
3. S. T. Thurman and J. R. Fienup, J. Opt. Soc. Am. A **25**, 995 (2008).
4. J. C. Marron, R. L. Kendrick, N. Seldomridge, T. D. Grow, and T. A. Hoft, Opt. Express **17**, 11638 (2009).
5. A. E. Tippie and J. R. Fienup, Opt. Lett. **34**, 701 (2009).
6. A. E. Siegman, *Lasers* (University Science Books, 1986).
7. R. A. Muller and A. Buffington, J. Opt. Soc. Am. **64**, 1200 (1974).
8. U. Grenander, *Abstract Inference* (Wiley, 1981).